Optical and radio observations of a sample of 52 powerful ultra-steep spectrum radio sources

C. Ledoux, J. Melnick, E. Giraud, Vainatey Kulkarni, B. Altieri

▶ **To cite this version:**

C. Ledoux, J. Melnick, E. Giraud, Vainatey Kulkarni, B. Altieri. Optical and radio observations of a sample of 52 powerful ultra-steep spectrum radio sources. Astronomy and Astrophysics - A&A, 2005, 436, pp.457-464. 10.1051/0004-6361:20052682 . in2p3-00025714

HAL Id: in2p3-00025714
https://hal.in2p3.fr/in2p3-00025714

Submitted on 21 Nov 2006

HAL is a multi-disciplinary open access archive for the deposit and dissemination of scientific research documents, whether they are published or not. The documents may come from teaching and research institutions in France or abroad, or from public or private research centers.

L'archive ouverte pluridisciplinaire **HAL**, est destinée au dépôt et à la diffusion de documents scientifiques de niveau recherche, publiés ou non, émanant des établissements d'enseignement et de recherche français ou étrangers, des laboratoires publics ou privés.

A&A 436, 457–464 (2005)
DOI: 10.1051/0004-6361:20052682
© ESO 2005

Astronomy & Astrophysics

Optical and radio observations of a sample of 52 powerful ultra-steep spectrum radio sources⋆,⋆⋆

Gopal-Krishna[1], C. Ledoux[2], J. Melnick[2], E. Giraud[3], V. Kulkarni[1], and B. Altieri[4]

[1] National Centre for Radio Astrophysics, TIFR, Post Bag 3, Ganesh Khind, Pune 411 007, India
e-mail: krishna@ncra.tifr.res.in; kulkarni@ncra.tifr.res.in
[2] European Southern Observatory, Alonso de Córdova 3107, Casilla 19001, Vitacura, Santiago, Chile
e-mail: cledoux@eso.org; jmelnick@eso.org
[3] GAM, Univ. Montpellier II, Place E. Bataillon, 34095 Montpellier Cedex, France
e-mail: edmond.giraud@gamum2.in2p3.fr
[4] European Space Agency, Villafranca del Castillo, Apartado 50727, 28080 Madrid, Spain
e-mail: baltieri@xmm.vilspa.esa.es

Received 12 January 2005 / Accepted 22 February 2005

Abstract. We present the results of radio (VLA) and optical (ESO/La Silla) imaging of a sample of 52 radio sources having an ultra-steep radio spectrum with α mostly steeper than -1.1 at decimetre wavelengths (median $\alpha = -1.22$). Radio-optical overlays are presented to an astrometric accuracy of $\sim 1''$. For 41 of the sources, radio spectral indices are newly determined using unpublished observations made with the 100-m Effelsberg radio telescope. For 14 of the sources identified with relatively brighter optical counterparts, spectroscopic observations were also carried out at La Silla and their redshifts are found to lie in the range 0.4 to 2.6. These observations have revealed three distant clusters of galaxies with redshifts of 0.55, 0.75 and 0.79, and we suggest that, together with an ultra-steep radio spectrum and relaxed radio morphology, the presence of a LINER spectrum in the optical can be used as a powerful indicator of rich clusters of galaxies. Additional candidates of this type in our sample are pointed out. Also, sources exhibiting particularly interesting radio-optical morphological relationships are highlighted. We further note the presence of six sources in our sample for which the optical counterpart (either detected or undetected) is fainter than $R \sim 24$ and the radio extent is small ($<10''$). These ultra-steep spectrum radio sources are good signposts for discovering massive galaxies out to very large redshifts.

Key words. cosmology: observations – galaxies: active – cooling flows – galaxies: clusters: general – quasars: general – radio continuum: galaxies

1. Introduction

The discovery of a correlation between the output of radio galaxies in optical emission lines and the radio band (e.g., Rawlings & Saunders 1991; McCarthy 1993) led to the recognition of using radio source samples as a means to detect galaxies located at very large distances. Indeed, radio surveys backed up with optical spectroscopy provided the first detections of objects beyond a redshift of two (e.g., Spinrad 1986). A major technical breakthrough came with the demonstration of a statistical correlation between radio spectral index and distance (Chambers et al. 1987; McCarthy et al. 1987), as already hinted in some earlier studies (e.g., Tielens et al. 1979; Blumenthal & Miley 1979; Gopal-Krishna et al. 1980; Gopal-Krishna & Steppe 1981). This correlation is now understood to be largely the result of a radio K-correction operating on the integrated spectrum which usually has a downward curvature arising from radiative losses (Laing & Peacock 1980). Consequently, the radio spectrum in a given frequency range appears increasingly steeper with redshift. The most distant radio galaxy found so far using the clue of ultra-steep radio spectrum has a redshift $z = 5.2$ (Venemans et al. 2004).

The spectacular success of using ultra-steep spectrum radio sources (hereafter USSRS) to discover high-z galaxies, from mid-80s to early 90s, later faced a stiff competition from a purely optical technique which involved multi-color photometry (Steidel et al. 1996). Nonetheless, the radio technique continues to offer at least two unique advantages. Firstly, the high-z galaxies thus found belong to the most massive stellar systems existing at their redshifts; this is particularly relevant for cosmological theories of structure formation (e.g., De Breuck et al. 2002; Lilly & Longair 1984). Secondly,

⋆ Based on observations carried out at the European Southern Observatory (ESO) on Cerro La Silla, Chile.
⋆⋆ Tables 1–3 and full Fig. 1 are only available in electronic form at http://www.edpsciences.org

Article published by EDP Sciences and available at http://www.edpsciences.org/aa or http://dx.doi.org/10.1051/0004-6361:20052682

an eventual discovery of radio sources beyond $z = 6$ would provide a direct probe of the "re-ionization era", via H I spectroscopy (e.g., Djorgovski et al. 2001). In this context, finding USSRS whose optical counterparts remain undetected down to fairly deep magnitudes ("empty fields") is particularly important. Moreover, from the astrophysical perspective, it is also of great interest to detect optical emission associated with the lobes and hot spots of radio galaxies at high redshifts where inverse Compton losses against the intense cosmic microwave background would severely limit the range of the electrons capable of optical synchrotron radiation (e.g., Brunetti et al. 2003; Gopal-Krishna et al. 2001).

In this paper, we present radio and optical imaging data for a sample of 52 USSRS (Sects. 2 and 3). Redshift measurements for the brighter subset of 14 sources are also presented. The radio maps are based on our Very Large Array (VLA) observations while the optical data were obtained using the telescopes of the European Southern Observatory (ESO) at La Silla.

2. Observations

2.1. The USSRS sample and radio imaging

The present sample of 52 USSRS with $\alpha < -1.05$ (but mostly <-1.1; see Table 1) is an assortment derived from the following four data-sets:

- The lists six to ten of the Ooty lunar occultation survey at 327 MHz (Subrahmanya & Gopal-Krishna 1979; Singal et al. 1979; Venugopal & Swarup 1979; Singal 1987): these are marked with "(oo)" in Table 1. Following Kühr et al. (1981), we have increased the published 327 MHz flux densities by 9%. To determine the radio spectral indices we have used these readjusted 327 MHz flux densities, but, if the source also appears in the 408 MHz Molonglo Reference Catalogue (MRC; Large et al. 1981) we instead used the 408 MHz flux from MRC. At high frequency, the fluxes are determined from the "cross-scan" observations of the Ooty sources at 2.7 GHz with the 100-m Effelsberg radio telescope (Kulkarni et al. 2005, in prep.). Note that for the source 2222−057 the Ooty flux at 327 MHz (Table 1) is only about half of the 1.03 Jy given in the 365 MHz Texas survey (Douglas et al. 1996). In view of this unusually large discrepancy, we have used in Table 1 the average of the two spectral indices determined using the Ooty and the Texas flux densities. This metre-wavelength flux averaging still leaves a large uncertainty of ±0.2 in the computed spectral index of −1.16 (Table 1).
- The Molonglo surveys MC 1 and MC 2 at 408 MHz (Davies et al. 1973; Sutton et al. 1974), marked with "(ml)" in Table 1: the spectral indices are derived by combining these Molonglo observations with the 2.7 GHz observations made with the Effelsberg telescope (Steppe & Gopal-Krishna 1984), or in two cases of positive declinations (MC 2), using the Green-Bank 300-ft dish (Murdoch 1976).
- The MIT-Green Bank (MG) survey (Lawrence et al. 1986): these sources are marked with "(mg)" in Table 1. For all these sources, the low-frequency flux densities are taken from the 408 MHz Molonglo Reference Catalogue (MRC). At high frequency, the flux densities are taken from the 4.8 GHz measurements reported in the MG survey using the Green-Bank 300-ft telescope. For one source, 1523−017, the spectral index is −1.04, which is slightly flatter than the nominal limit of our sample, $\alpha = -1.05$.
- Finally, a small number of the sources, marked with "(gb)", were picked by comparing the Molonglo Reference Catalogue at 408 MHz with *A 1400 MHz Sky Atlas* distributed by NRAO (USA; J.J. Condon & J.J. Broderick). On the high frequency side, we have used the 4.8 GHz measurements made with the Green-Bank 300-ft dish (Becker et al. 1991, or Gregory & Condon 1991). For three of the sources, which are not covered in these 4.8 GHz surveys, we have used the 1.4 GHz flux values either from the NVSS (Condon et al. 1998) or the Green-Bank Survey (White & Becker 1992).

It may be noted that since the sizes of practically all sources in our sample are well within one arcmin, any underestimation of their flux densities should be negligible, given that the measurements are based either on lunar occultation records, or made using pencil beams of size ∼5 arcmin, to within a factor of two (see the comments in Sect. 3 for 1005−046 which is the only source in our sample whose size is larger than one arcmin).

For all sources in our sample, except those few for which VLA maps at 4.8 GHz (A-array) were available in Bennett et al. (1986), we took five to ten minutes snapshots using the VLA at 4.8 GHz. The majority of these observations were made in the BnC hybrid configuration while the DnC array was used in the remaining cases. The data restoration was done using the AIPS package (details will be given in Kulkarni et al. 2005, in prep.). The derived radio images are shown as overlays in Fig. 1 while the main structural parameters are given in Table 1.

2.2. Optical imaging

The optical observations were taken during several observing runs between 1989 and 1996 using telescopes at La Silla. The bulk of the data was obtained in the period 1989–1991 using EFOSC 1 at the La Silla 3.6 m telescope. Standard Bessel *BVRI* filters were used at all observing runs, and both imaging and spectroscopy were performed using EFOSC-type instruments. The characteristics of these instruments is summarized in Tables 2 and 3, that condense the relevant information from successive generations of User's Manuals. The data reduction was performed using MIDAS, the data reduction and analysis software developed at ESO. Most observations were taken under reasonably good seeing conditions (at least by the standards of those days) ranging between one and 1.″5, with little or no moon illumination. However, the observations of the sources 0001+058, 2232−062, 2236−039 and 2245−037 were made on a bright moonlit night with rather poor seeing conditions (∼2″). Consequently, the detection limit attained for these

Article published by EDP Sciences and available at http://www.edpsciences.org/aa or http://dx.doi.org/10.1051/0004-6361:20052682

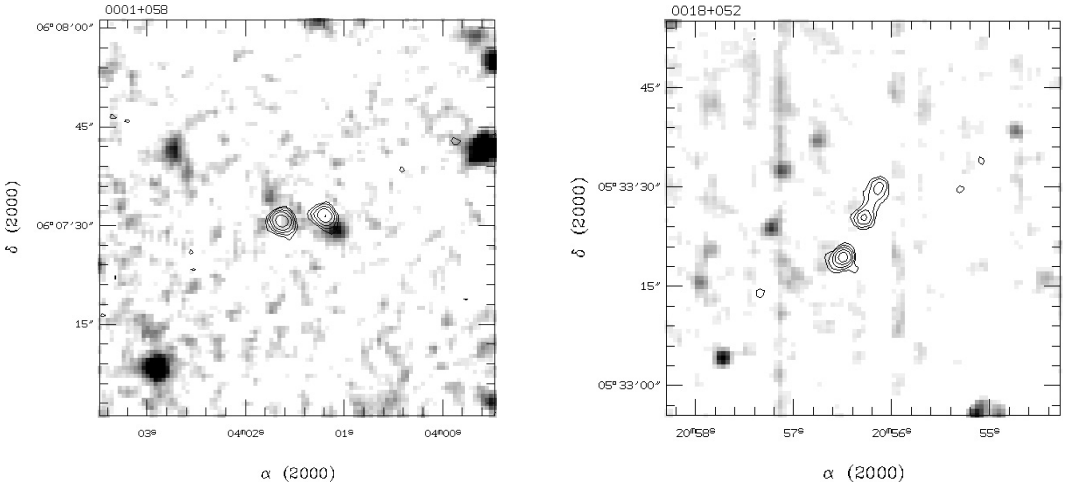

Fig. 1. Radio-optical overlays. The insets show the optical counterparts without radio contour. The radio contours are based on VLA snapshots taken at 4.8 GHz.

fields is only around $R \sim 23$. The optical and radio images are shown in Fig. 1 when not already published elsewhere.

2.3. Astrometry

We began by determining positions for three to five secondary reference stars near the radio positions using stars from the SAO catalogue. To do this, we prepared contact glass plate copies of the fields from the Red POSS prints. The positions of the primary and secondary reference stars on these contacts were measured using a Zeiss *X*-*Y* measuring machine. This allowed us to determine the positions of the secondary reference stars to a typical accuracy of 1″ or better using a least-squares solution of the transformation equations. Then, for each pair of secondary reference stars visible on the CCD frames, we determined the scale and orientation of the image and the position of the radio source. The final position of the radio source was determined by averaging the positions estimated using all the available pairs of secondary reference stars in each image. The scatter in the derived positions was typically between one and 2″; hence, the expected astrometric accuracy is ∼1″ rms. For about 40% of the sample, however, only two reference stars were present on the CCD frames. For these objects, we estimate the positional accuracy to be within one and 2″ rms based on our experience for the rest of the sample. If the two stars are located on opposite sides of the radio position and neither is saturated, the astrometric accuracy is ∼1.″5 rms (class "b" in the last column of Table 1). Otherwise, the astrometry has ∼2″ rms error (class "c"). The remaining ∼60% of the sample has at least three reference stars and the astrometric accuracy is ∼1″ rms (class "a").

We emphasize that, by itself, the astrometric error class can be treated as the principal reliability indicator of optical identification only provided the radio source is compact (smaller than ∼5″), or it contains a compact central radio component. For extended radio sources larger than ∼10″ and lacking a central component, offsets of up to ∼25% of the size of the radio source, between the optical identification and the radio centroid, can be accepted.

2.4. Photometry

Direct imaging observations were not always obtained under photometric conditions, although, due to the faintness of the sources, rather good transparency was always required. Not all observations, therefore, were photometrically calibrated. On photometric nights, calibrations were done using several stars from the Landolt (1992) CCD fields. Given the excellent photometric stability of the EFOSC instruments, we were able to determine the magnitudes of the objects observed under non-photometric conditions using the standard zero points given in the User's Manuals. Due to the unknown atmospheric extinction, however, these magnitudes carry rather large observational errors (in some cases even up to 0.5 mag).

To determine the magnitudes of the optical counterparts of the radio sources, we followed two procedures. For most objects, we carried out circular aperture photometry with adequate aperture size (using the MIDAS software) whereas for objects located in crowded/confused regions we additionally employed the SExtractor algorithm (Bertin & Arnouts 1996) to deblend the different close-by objects. Each of these procedures gives a magnitude estimate with an associated error. These values are reflected in the estimates given in Table 1. It should be stressed that additional uncertainties can be expected due to systematic effects, mainly non-photometric conditions (see above). For blank fields, a 3σ lower limit to the magnitude was determined by circular aperture photometry taking the radius to be equal to the mean FWHM of several stars on the same CCD frame.

2.5. Redshifts

Whenever optical identification could be established and weather conditions allowed, we used the available telescope time to obtain spectra of the sources using the identification

Article published by EDP Sciences and available at http://www.edpsciences.org/aa or http://dx.doi.org/10.1051/0004-6361:20052682

images to place the slit on the objects. Otherwise, we performed the source identifications off-line, and carried out spectroscopy subsequently on any available nights. In spite of considerable efforts, however, the number of sources for which we were able to obtain redshifts remains rather small and for several sources the spectroscopy did not yield redshift (these sources are marked with an asterisk in the last column of Table 1). Plausibly, this is due to the fact that, due to the high read-out noise and low blue sensitivity of the CCDs of those days, our ability to detect Lyα emission in the range $1.8 < z < 2.3$ was rather limited, while powerful radio sources tend to cluster at redshifts between one and two (see, e.g., Condon 2003).

3. Comments on individual systems

3.1. 0001+058

The optical identification is a fuzzy object close to the detection limit situated between the two radio lobes. An object of $R = 22.7 \pm 0.3$ is located about 4″ to the SW of the western lobe. Another close-by, much fainter object ($R = 23.2 \pm 0.4$) is seen about 5″ North of the eastern lobe.

3.2. 0018+052

It cannot be entirely excluded that the optical identification of this radio source is not located on a bad CCD column. For this reason, the source remains undetected down to $R = 23$.

3.3. 0030+061

This is a clear empty field since no optical object is visible within a radius of 6″ from the radio source.

3.4. 0048+072

The optical field without radio contours is shown in the inset of the overlay in Fig. 1. A faint object with $R = 21.9 \pm 0.1$ seen at the centre of the inset, which coincides with the mid-point of the two radio lobes, is a likely identification. Another candidate is the brighter object with $R = 20.8 \pm 0.1$ situated ∼4″ NW of the radio centre.

3.5. 0127−195

This radio source is located in a clear empty field.

3.6. 0321−042

The R-band overlay image shown in Fig. 1 has been taken with EFOSC 2 at the NTT which has a higher resolution than the B-band image used for the photometry (see Table 1). The optical identification, more clearly seen in the inset of the overlay, is a QSO with redshift $z = 2.53$ based on prominent broad Lyα and C IV lines.

3.7. 0348+013

The hint of a wide-angle-tail radio morphology signifies the presence of a cluster. Interestingly, the optical counterpart is a QSO with redshift $z = 1.12$ based on several emission lines visible in our spectra. About 9″ to the SW of the quasar, a foreground elliptical galaxy is seen for which we find a redshift $z = 0.27$. The R-band image shown in Fig. 1 has been taken with EFOSC 2 at the NTT which has a higher resolution than the R-band image used for the photometry.

3.8. 0355−037

The R-band overlay image shown in Fig. 1 resulted from a 30 min exposure taken with EFOSC 2 at the NTT which has a higher resolution than the R-band image used for the photometry (see Table 1). The optical ID lies closer to the eastern lobe of the radio source. It has a fuzzy appearance, roughly extended along the radio axis. It has a northward extension of 5″, which is also seen on the EFOSC 1 image used for the photometry. It could possibly be a chain of fainter galaxies, or even a tidal tail resulting from a merger event.

3.9. 0410−198

Our results for this source are published in Giraud et al. (1996a). It is identified with the dominant galaxy of a $z = 0.79$ cluster. A remarkable optical extended emission-line region (EELR) of low excitation and size, ∼100 kpc, was found associated with the radio galaxy. The EELR bears a close morphological relationship to the radio lobes which exhibit Z-shaped symmetry. The EELR appears to consists of three cones associated with the radio galaxy and a neighbouring galaxy also located at the same redshift and connected to the former by a long stellar filament.

3.10. 0423−199

The optical counterpart is clearly extended along the two radio lobes (see inset in Fig. 1). Our low-dispersion spectra yielded a redshift $z = 1.12$ based on three (narrow?) emission lines (C III] λ1909, Mg II λ2800, [O II] λ3727).

3.11. 0424−197

An almost point-like object lies at the position of this barely resolved radio source.

3.12. 0430−197

Only a pointing optical image (3 min exposure) is available for this small diameter radio source which remains unidentified down to $R = 22.7$. A deeper image is needed.

3.13. 0441+049

The optical counterpart is a diffuse object with two peaks separated by 2″ along the radio axis.

Article published by EDP Sciences and available at http://www.edpsciences.org/aa or http://dx.doi.org/10.1051/0004-6361:20052682

3.14. 0449−195

The optical counterpart of this marginally resolved radio source is not visible in our 3 min pointing image. A deeper image is needed for this source.

3.15. 0551−196

A galaxy of $R = 22.3 \pm 0.2$ which is seen at the centre of the overlay is situated roughly midway between the two widely separated radio "lobes". This is a possible identification. However, since the southern lobe is itself resolved into two components, it is possible that the two lobes are in fact independent radio sources. In that event, their optical counterparts are undetected down to $R = 23.7$.

3.16. 0634−196

This barely resolved radio source is a clear empty field located towards the Galactic anticentre ($b = -12.4°$).

3.17. 0852+124

Our results for this source are published in Gopal-Krishna et al. (1995). A giant cloud of Lyα emission at $z = 2.468$ extended over ∼100 kpc is associated with the southern radio lobe. The equivalent width of Lyα is exceptionally large (∼1000 Å in the rest-frame) and the line profile indicates expansion at a velocity of ∼550 km s^{-1}, probably driven by the radio lobe from within. The Lyα emission shows a sharp cut-off near the radio galaxy indicative of a dusty disc around the galaxy, oriented roughly perpendicular to the radio axis.

3.18. 0918−194

The only optical object detected between the two radio lobes is a galaxy at $\alpha = 09^{\rm h}21^{\rm m}15.7^{\rm s}$, $\delta = -19°37'43''$ (J 2000).

3.19. 0946+077

The optical counterpart of this small diameter (3″) radio source is below the detection limit in our image, $R > 23.3$. There is a bright object about 7″ West of the radio position.

3.20. 1005−046

Since our VLA map shows the size of this source to be 100″, its flux density given in the Molonglo Reference Catalogue at 408 MHz (MRC does not give integrated flux) might be significantly underestimated. Hence we have computed the spectral index using the flux densities estimated from the NVSS map (353 mJy at 1.4 GHz) and the Parkes survey (87 mJy at 4.85 GHz; Griffith et al. 1995). We further note that our VLA map shows a prominent radio core in this triple source, which contributes ∼9 mJy at 4.85 GHz.

The optical identification is a bright, narrow emission-line radio galaxy (NELG) at a redshift $z = 0.618$. A close inspection of the image shows that the optical counterpart could be a tight chain of three objects. The southern radio hot spot coincides with a point-like optical object with $R = 19.7 \pm 0.1$.

3.21. 1048+002

The optical identification lies closer to the northern radio lobe and is seen more clearly near the centre of the inset. After 4 h of integration, the optical spectrum shows two narrow faint emission lines that we tentatively identify with Mg II λ2800 and [O II] λ3727 at $z = 0.71$. Note also that a faint optical object is coincident with the outer edge of the southern radio lobe.

3.22. 1059+107

The optical ID is a galaxy that coincides with the central radio component and is elongated along the radio axis. A relatively bright star is located 6″ to the SE of the galaxy.

3.23. 1132+112

The optical ID of this radio source is a point-like object with $R = 22.0 \pm 0.1$.

3.24. 1146+052

The best candidate for optical identification is a $R = 22.6 \pm 0.1$ galaxy situated at $\alpha = 11^{\rm h}48^{\rm m}47.9^{\rm s}$, $\delta = +04°55'25''$ (J 2000). It could be the dominant member of a distant cluster. Our 2 h spectrum of this galaxy shows a strong [O II] λ3727 emission line and a rich Balmer absorption spectrum, reminiscent of other cluster sources (Melnick et al. 1997). Unfortunately, our B 300 spectra cuts off just where we would expect to see the [O III] emission lines at $z = 0.42$, so we cannot be certain of the LINER nature of this source.

3.25. 1224−085

The identified optical structure consists of a $R = 23.5 \pm 0.3$ point-like object and a faint, 6″ long wisp to SW coincident with the southern radio lobe and elongated along the radio axis. The entire structure has $R \sim 22$.

3.26. 1238−074

The radio structure is poorly resolved in our low-resolution VLA map. The only object within 5″ of the radio peak is a $R \sim 23$ fuzzy object situated at $\alpha = 12^{\rm h}40^{\rm m}48.0^{\rm s}$, $\delta = -07°43'18''$ (J 2000).

3.27. 1245+115

The likely optical counterpart is a point-like object located 6″ NW of a bright star.

Article published by EDP Sciences and available at http://www.edpsciences.org/aa or http://dx.doi.org/10.1051/0004-6361:20052682

3.28. 1246−081

The optical counterpart of this slightly resolved (∼1″) radio source is a $R = 22.8 \pm 0.4$ object. A fainter object is also seen 2″ NE of it.

3.29. 1248−108

The central radio component lies within 1.″5 of a pair of optical objects which are themselves separated by 2″ and have an integrated $R = 22.7 \pm 0.3$. One of these objects is the likely optical ID.

3.30. 1317−194

An object of $R = 24.4 \pm 0.2$ is seen 1.″5 NE of the central component of this extended radio source. The astrometry has been independently checked using a 10 min exposure taken with EFOSC 1 at the ESO 3.6 m telescope. This image is less deep but includes five reference stars and confirms the astrometry as shown in the overlay.

3.31. 1324−104

The likely optical ID is close to the north-eastern radio lobe and appears to be extended.

3.32. 1329−195

An optical object is seen about 2.″5 offset from the radio peak towards NE. Within the astrometric uncertainties for this case, this object is the likely identification. Faint and narrow emission lines of [C II] λ2326 and Mg II λ2800 are visible in our 2 h spectrum of this object indicating that the radio source is probably a NELG at a redshift $z = 0.98$.

3.33. 1411−192

Our results for this source are published in Gopal-Krishna et al. (1992). An EELR of size ∼100 kpc and $z = 0.477$ is associated with this double radio source. Its [O II] λ3727 emission line has a very large rest-frame equivalent width (350 Å), consistent with the high radio luminosity. Intriguingly, we found that its optical spectrum is ultra-soft, with [O II] λ3727/[O III] λ5007 = 10, nearly 30 times the typical value for distant 3CR radio galaxies (van Breugel & McCarthy 1990). Together with Hydra A, this source thus provides an outstanding example of extremely low-ionization optical emission-line spectra being associated with powerful radio galaxies (Melnick et al. 1997). Unfortunately, the object is seen very close to a bright star, so it is difficult to say whether it is a cluster source like Hydra A.

3.34. 1443−198

Deep multi-color optical observations of this source have been reported by us (Giraud et al. 1996b). The source was identified with a $z = 0.753$ elliptical galaxy in the process of formation by accreting material from neighbouring galaxies, all members of a group. The radio source has a central core and two relatively relaxed lobes consistent with its being in a cluster.

3.35. 1509−158

The peak of this unresolved radio source lies just ∼15″ from a pair of bright stars. No optical identification is visible above a detection limit of $R \sim 24$. The radio flux measurement at 2.7 GHz (Effelsberg) contains a significant contribution from a 10″ double radio source located 2.′8 to the NW of 1509−158. Due to this, the true spectral index of this source is probably even steeper than the −1.24 value given in Table 1. The parameters of the confusing source, estimated from our VLA observations, are $\alpha = 15^{\rm h}12^{\rm m}22.7^{\rm s}$, $\delta = -15°58'05''$ (J 2000), with a flux density equal to 36 mJy at 5 GHz (Kulkarni et al. 2005, in prep.).

3.36. 1523−017

The radio map of this triple source is taken from the VLA 5 GHz observations by Bennett et al. (1986). The redshift of the optical counterpart, $z = 0.93$, was derived from a 3 h low-dispersion (B 1000) spectrum taken with EFOSC 1. The spectrum shows prominent, probably narrow, Mg II and [O II] emission lines. The presence of H+K in absorption and the lack of strong [O III] emission lines indicate that this object may be a LINER.

3.37. 1612−208

The optical counterpart of this unresolved radio source is quite bright and point-like. The blue spectrum of this object obtained from 2 h integration with EFOSC 1 is typical of an elliptical galaxy at $z = 0.31$. The lack of emission lines and the compactness of the object, however, are rather puzzling.

3.38. 1621−196

Although this object has a large radio size, its optical identification remains uncertain. The nearest object to the radio centre is a $R = 21.6 \pm 0.2$ point-like object, which we suggest as the possible identification. However, it is offset by 4″ to the South of the faint radio peak seen between the two radio lobes. In addition to the R-band photometry, we also took a 15 min V-band exposure using EFOSC 1 from which we get $V = 21.2 \pm 0.1$ and $V - R = -0.4$ assuming that the object did not vary over the 11 months time interval between the two observations. If a higher resolution radio map confirms the faint, central peak to be the radio nucleus then its separation from the suggested optical ID would be four times the rms astrometric error. Any other optical ID would have to be below the detection limit of the image ($R \sim 25$ for a point source).

3.39. 1623−194

The optical counterpart of this radio source is a point-like object.

Article published by EDP Sciences and available at http://www.edpsciences.org/aa or http://dx.doi.org/10.1051/0004-6361:20052682

3.40. 1631−222

The source lies in a crowded field close to the Galactic plane (latitude +16°). The only detected object within 2″ is a R = 25.5 ± 0.4 object located about 2″ North of the radio peak. This is the likely optical ID for this unresolved radio source.

3.41. 1632−199

This compact steep spectrum radio source lies in a clear empty field.

3.42. 1859−187

This extended radio source lies in a crowded field close to the Galactic plane (latitude −10.7°). The inset shows five bright objects near the mid-point between the two radio lobes. Of these, the western-most object, which is slightly extended, is the most likely optical identification.

3.43. 2011−169

The optical counterpart of this compact steep spectrum radio source is undetected down to a very deep level (R = 25.6).

3.44. 2023−156

There is a hint of a central radio component. The NS extended optical object is offset from this component by 1.″5 to the North, which is within the astrometric error, and is therefore the likely optical counterpart.

3.45. 2057−179

The suggested optical ID partially overlaps with the image of a 1.6 mag brighter elliptical galaxy located about 3″ to the South. A 2 h spectrum obtained with EFOSC 2 at the ESO/MPI 2.2 m telescope shows a rich emission-line spectrum at z = 0.92. The adjacent elliptical galaxy is at z = 0.6.

3.46. 2105−119

The best candidate appears to be the slightly extended object located about 1.″3 West of the radio position. A very faint fuzz is coincident with the radio peak.

3.47. 2222−057

The spectral index of this radio source has a large uncertainty of ±0.2 (see Sect. 2.1). No object is seen within the radio contours above the detection limit of the image ($R \sim 23$).

3.48. 2232−062

A tight clustering of bright stars is seen within 20″ West of this radio source. This considerably degrades the quality of detection of the faint ($R \sim 23.5$) optical counterpart observed between the two radio lobes.

3.49. 2236−039

This compact steep-spectrum radio source coincides with a barely detected fuzz with $R \sim 23$ situated in a crowded field.

3.50. 2236−047

The results of our detailed optical observations of this source have been reported by Melnick et al. (1993). The distorted double radio source is identified with a z = 0.552 cD galaxy which is member of a cluster (Kulkarni et al. 2005, in prep.). Between this galaxy and another similarly bright galaxy to the NE, which is a member of the same cluster, an unusually bright and straight arc-like feature was found by Melnick et al. (1993). We interpreted it as the image of a pair of merging galaxies at z = 1.116, highly magnified due to gravitational lensing by the foreground cluster (see also Kneib et al. 1994).

3.51. 2245−037

On the assumption that the two radio components of this source are physically associated, the most likely optical identification is the bright (R = 20.8 ± 0.1) object roughly located midway between them. On the other hand, it is quite possible that the two radio components are independent radio sources (particularly since the western component is itself a 6″ double). In that case, the optical features detected towards each of them would be their likely optical IDs. The magnitudes of these objects are R = 22.7 ± 0.2 for the western lobe and R = 20.8 ± 0.1 for the source close the eastern lobe.

3.52. 2347+015

More sensitive radio imaging is needed to confirm if this source is a wide-angle tail. The likely optical identification is coincident with the radio peak.

4. Conclusions

We have presented a catalogue of 52 powerful radio sources with very steep spectra at decimetre wavelengths (median α = −1.22). For ∼15% of the sources, the observing conditions were poor or the optical fields are confused, so even if the optical counterparts may not be very faint, they could not be identified with the available material. Out of the 41 (i.e., ∼80%) identified sources, in spite of considerable efforts, we were also able to obtain redshifts for only about a third of them. This is most likely due to the fact that the CCDs of those days had rather high read-out noise and poor blue sensitivity. We are confident that using modern detectors *on the same telescopes* we should be able to do a lot better.

Our sample is found to contain six USSRS that are not only optically very faint ($R \gtrsim 24$) but also have small radio sizes (<10″). These sources, namely, 0001+058, 0634−196, 1509−158, 1631−222, 2011−169 and 2105−119, are prime candidates to be at very large redshifts, and indeed, we plan to make a new round of optical identifications to complete the catalogue.

Article published by EDP Sciences and available at http://www.edpsciences.org/aa or http://dx.doi.org/10.1051/0004-6361:20052682

Finally, we note that, even though optical spectroscopy has been completed for only about a quarter of the sample (14 sources), already this small subset is found to contain two powerful ultra-steep spectrum radio sources having LINER-type ultra-soft emission-line spectra (0410−198 and 1411−192 at, respectively, $z = 0.79$ and 0.48) plus at least one good candidate (1523−017 at $z = 0.93$). Another three candidates, namely, 0423−199 ($z = 1.12$), 1146+052 ($z = 0.42$) and 2057−179 ($z = 0.92$), show strong [O II] emission but since their existing spectra do not extend to the region of the [O III] line, spectral softness based on the strengths of these two emission lines remains to be confirmed. Our observations indicate that the former two sources are associated with distant ($z \gtrsim 0.5$) galaxy clusters having a dense intra-cluster medium, as is the case for the nearby massive cooling flow cluster Hydra A (Melnick et al. 1997; also, McNamara 1995). Thus, together with an ultra-steep radio spectrum and relaxed radio morphology, the presence of a LINER spectrum in the optical can be used as a powerful indicator of high-z clusters which are not merely concentrations of galaxies, but have acquired an intra-cluster medium dense enough to sustain cooling flow activity.

Acknowledgements. G.K. thanks ESO for the hospitality in Chile during a visit when this project was started. JM thanks NCRA, Pune, for their hospitality when this project was finished. We also thank Samir Dhurde and Alok Gupta for their invaluable help with data handling. This work made use of the MIDAS and AIPS data reduction and analysis packages as well as the NASA/IPAC extragalactic database (NED). VLA is operated by Associated Universities, Inc., under contract with the National Science Foundation.

References

Becker, R. H., White, R. L., & Edwards, A. L. 1991, ApJS, 75, 1
Bennett, C. L., Lawrence, C. R., Burke, B. F., Hewitt, J. N., & Mahoney, J. 1986, ApJS, 61, 1
Bertin, E., & Arnouts, S. 1996, A&AS, 117, 393
Blumenthal, G., & Miley, G. 1979, A&A, 80, 13
Brunetti, G., Mack, K.-H., Prieto, M. A., & Varano, S. 2003, New A Rev., 47, 501
Chambers, K. C., Miley, G. K., & van Breugel, W. 1987, Nature, 329, 604
Condon, J. J. 2003, in Radio Astronomy at the Fringe, ed. J. A. Zensus, M. H. Cohen, & E. Ros, San Francisco, CA, ASP Conf. Proc., 300, 243
Condon, J. J., Cotton, W. D., Greisen, E. W., et al. 1998, AJ, 115, 1693
Davies, I. M., Little, A. G., & Mills, B. Y. 1973, Aust. J. Phys. Astrophys. Suppl., 28, 1
De Breuck, C., van Breugel, W., Stanford, S. A., et al. 2002, AJ, 123, 637
Djorgovski, S. G., Castro, S., Stern, D., & Mahabal, A. A. 2001, ApJ, 560, L5
Douglas, J. N., Bash, F. N., Bozyan, F. A., Torrence, G. W., & Wolfe, C. 1996, AJ, 111, 1945
Giraud, E., Melnick, J., Gopal-Krishna, Mendes de Oliveira, C., & Kulkarni, V. K. 1996a, A&A, 309, 733
Giraud, E., Melnick, J., Gopal-Krishna, & van Drom, E. 1996b, A&A, 311, 446
Gopal-Krishna, Giraud, E., Melnick, J., & della Valle, M. 1995, A&A, 303, 705
Gopal-Krishna, Giraud, E., Melnick, J., & Steppe, H. 1992, A&A, 254, 42
Gopal-Krishna, & Steppe, H. 1981, A&A, 101, 315
Gopal-Krishna, Steppe, H., & Witzel, A. 1980, A&A, 89, 169
Gopal-Krishna, Subramanian, P., Wiita, P. J., & Becker, P. A. 2001, A&A, 377, 827
Gregory, P. C., & Condon, J. J. 1991, ApJS, 75, 1011
Griffith, M. R., Wright, A. E., Burke, B. F., & Ekers, R. D. 1995, ApJS, 97, 347
Kneib, J. P., Melnick, J., & Gopal-Krishna 1994, A&A, 290, L25
Kühr, H., Witzel, A., Pauliny-Toth, I. I. K., & Nauber, U. 1981, A&AS, 45, 367
Laing, R. A., & Peacock, J. A. 1980, MNRAS, 190, 903
Landolt, A. U. 1992, AJ, 104, 340
Large, M. I., Mills, B. Y., Little, A. G., Crawford, D. F., & Sutton, J. M. 1981, MNRAS, 194, 693
Lawrence, C. R., Bennett, C. L., Hewitt, J. N., et al. 1986, ApJS, 61, 105
Lilly, S. J., & Longair, M. S. 1984, MNRAS, 211, 833
McCarthy, P. J. 1993, ARA&A, 31, 639
McCarthy, P. J., Spinrad, H., Djorgovski, S., et al. 1987, ApJ, 319, L39
McNamara, B. R. 1995, ApJ, 443, 77
Melnick, J., Altieri, B., Gopal-Krishna, & Giraud, E. 1993, A&A, 271, L5
Melnick, J., Gopal-Krishna, & Terlevich, R. 1997, A&A, 318, 337
Murdoch, H. S. 1976, MNRAS, 177, 441
Rawlings, S., & Saunders, R. 1991, Nature, 349, 138
Singal, A. K. 1987, A&AS, 69, 91
Singal, A. K., Gopal-Krishna, & Venugopal, V. R. 1979, Mem. Astron. Soc. India, 1, 14
Spinrad, H. 1986, PASP, 98, 269
Steidel, C. C., Giavalisco, M., Pettini, M., Dickinson, M., & Adelberger, K. L. 1996, ApJ, 462, L17
Steppe, H., & Gopal-Krishna 1984, A&A, 135, 39
Subrahmanya, C. R., & Gopal-Krishna 1979, Mem. Astron. Soc. India, 1, 2
Sutton, J. M., Davies, I. M., Little, A. G., & Murdoch, H. S. 1974, Aust. J. Phys. Astrophys. Suppl., 33, 1
Tielens, A. G. G. M., Miley, G. K., & Willis, A. G. 1979, A&AS, 35, 153
van Breugel, W. J. M., & McCarthy, P. J. 1990, in Evolution of the Universe of Galaxies, San Francisco, CA, ASP Conf. Ser., 10, 359
Venemans, B. P., Röttgering, H. J. A., Overzier, R. A., et al. 2004, A&A, 424, L17
Venugopal, V. R., & Swarup, G. 1979, Mem. Astron. Soc. India, 1, 25
White, R. L., & Becker, R. H. 1992, ApJS, 79, 331

Article published by EDP Sciences and available at http://www.edpsciences.org/aa or http://dx.doi.org/10.1051/0004-6361:20052682

Online Material

Article published by EDP Sciences and available at http://www.edpsciences.org/aa or http://dx.doi.org/10.1051/0004-6361:20052682

Table 1. Overall properties of the sample galaxies⋆.

			Radio properties			Optical properties		
IAU name[1]	RA[2]	Dec[2]	Morphology[3]	α	Flux[4]	Magnitude	z	Observations[5]
	[J 2000]	[J 2000]	(Size)		[Jy]			
0001+058 (oo)	00 04 01.48	+06 07 31.0	D (∼7″)	–1.16	1.28	$R \sim 24$	...	I3, c
0018+052 (oo)	00 20 56.29	+05 33 25.4	T (12″)	–1.38	1.78	$R > 23.0$	...	I2, c
0030+061 (mg)	00 33 15.28	+06 28 18.0	R (3″)	–1.20	3.09	$R > 23.0$	...	I2, b
0048+072 (oo)	00 51 28.03	+07 28 55.4	D (20″)	–1.12	1.96	$R = 21.9 \pm 0.1$	...	I3, a
0127−195 (ml)	01 30 00.38	−19 17 11.1	SR (∼1″)	–1.41	0.30	$R > 23.0$	...	I2, b
0321−042 (gb)	03 24 21.03	−04 05 03.8	SR (∼1″)	–1.20	0.87	$B = 22.4 \pm 0.1$	2.53	I1, S3, S4, S6, a
0348+013 (gb)	03 50 57.37	+01 31 04.6	D (∼8″)	–1.20	1.02	$R = 18.9 \pm 0.1$	1.12	I1, S1, S2, S3, a
0355−037 (gb)	03 57 47.91	−03 34 07.9	D (12″)	–1.27	1.05	$R = 23.3 \pm 0.3$	...	I1, a
0410−198 (ml)	04 12 29.21	−19 42 08.8	D (11″)	–1.18	2.23	$R = 20.9 \pm 0.2$	0.79	published
0423−199 (ml)	04 25 44.33	−19 50 25.2	D (3″)	–1.25	0.92	$R = 23.1 \pm 0.2$	1.12	I2, S3, S6, a
0424−197 (ml)	04 26 37.62	−19 37 48.2	SR (∼1″)	–1.20	0.38	$R = 22.0 \pm 0.3$	...	I2, a, ∗
0430−197 (ml)	04 32 28.30	−19 40 45.2	R (2″)	–1.20	0.47	$R > 22.7$	...	I2, a
0441+049 (gb)	04 44 17.94	+05 01 25.6	D (12″)	–1.10	0.83	$R \sim 23$	...	I1, b
0449−195 (ml)	04 51 13.15	−19 29 11.3	SR (∼1″)	–1.22	0.24	$R > 23.3$	...	I1, a
0551−196 (ml)	05 53 11.06	−19 36 53.4	D? (34″)	–1.31	0.48	$R = 22.3 \pm 0.2$	...	I2, a, ∗
0634−196 (ml)	06 36 28.68	−19 38 47.2	SR (∼1″)	–1.24	0.60	$R > 24$	...	I2, a
0852+124 (oo)	08 55 21.37	+12 17 26.3	D (15″)	–1.28	1.05	$V = 23.3 \pm 0.4$	2.47	published
0918−194 (ml)	09 21 15.49	−19 37 37.4	D (29″)	–1.20	0.30	$R = 22.7 \pm 0.3$	...	I2, a
0946+077 (mg)	09 48 55.25	+07 28 09.2	R (5″)	–1.14	1.99	$R > 23.3$	...	I2, a
1005−046 (gb)	10 07 49.30	−04 53 42.0	T (100″)	–1.13	1.08	$R = 20.2 \pm 0.1$	0.62	I4, S1, a
1048+002 (gb)	10 50 40.35	−00 03 53.9	D (7″)	–1.22	3.46	$R = 22.3 \pm 0.2$	0.71	I2, S1, S4, a
1059+107 (gb)	11 02 17.42	+10 29 07.5	T (6″)	–1.42	3.50	$R = 21.9 \pm 0.1$	...	I4, b
1132+112 (ml)	11 35 21.10	+10 56 19.3	D (8″)	–1.26	0.97	$R = 22.0 \pm 0.1$	...	I6, a
1146+052 (mg)	11 48 47.78	+04 55 25.2	D (41″)	–1.13	2.65	$R = 22.6 \pm 0.1$	0.42	I4, S1, S3, S5, b
1224−085 (oo)	12 27 03.73	−08 48 26.7	D (7″)	–1.20	1.23	$R \sim 22$	...	I4, c, ∗
1238−074 (oo)	12 40 47.82	−07 43 13.9	SR (∼2″)	–1.12	(0.6)	$R = 23.3 \pm 0.3$	...	I6, a
1245+115 (ml)	12 48 17.16	+11 17 22.9	SR (∼2″)	–1.48	1.15	$R = 21.3 \pm 0.1$	...	I6, b
1246−081 (oo)	12 48 51.32	−08 22 27.7	SR (∼1″)	–1.37	(1.0)	$R = 22.8 \pm 0.4$	...	I2, a
1248−108 (oo)	12 50 40.00	−11 05 34.1	T (10″)	–1.36	(0.8)	$R = 22.7 \pm 0.3$	...	I2, a
1317−194 (ml)	13 20 11.83	−19 42 29.0	T (24″)	–1.22	0.23	$R = 24.4 \pm 0.2$	...	I4, a
1324−104 (oo)	13 26 47.77	−10 40 50.6	D (6″)	–1.28	(0.55)	$R = 22.3 \pm 0.2$	...	I2, b
1329−195 (ml)	13 31 47.13	−19 47 26.3	SR (∼2″)	–1.28	0.35	$R = 22.3 \pm 0.2$	0.98	I2, S1, b
1411−192 (oo)	14 14 22.97	−19 27 54.8	D (∼12″)	–1.27	1.33	$R \sim 22.6$	0.48	published
1443−198 (ml)	14 46 48.31	−20 03 38.0	D/T (7″)	–1.27	0.95	$R \sim 20.9$	0.75	published
1509−158 (oo)	15 12 31.02	−16 00 04.1	U (<5″)	–1.24	1.03	$R > 24$	...	I2, b

Notes:

⋆ Detailed information about each source is given in Sect. 3.

[1] The characters in parenthesis after the IAU names codify the radio survey from where the object was selected as follows: (oo) Ooty lunar occultation survey at 327 MHz; (ml) Molonglo surveys (MC 1 and MC 2) at 408 MHz; (mg) MIT (365 MHz) – Green-Bank (4.8 GHz) survey; (gb) Green-Bank (1.4 GHz) – Molonglo (408 MHz) survey.

[2] The positions refer to the radio peak for unresolved sources and to the central radio component if detected. For the remaining sources, the mid-point between the lobes is adopted (see Fig. 1).

[3] Radio morphology: D (Double), T (Triple), SR (Slightly Resolved), R (Resolved), U (Unresolved).

[4] The radio fluxes are given at 408 MHz, except the values in parenthesis that correspond to 327 MHz.

[5] The codes for the optical observations (I, S) are as defined in Tables 2 and 3. Exposure times for imaging ranged between ten and 30 min at the ESO 3.6 m/NTT 3.5 m telescopes, and 20 and 60 min at the ESO 2.2 m/Danish 1.5 m telescopes. Exposure times for spectroscopy are given together with the comments for each source. The letters "a", "b" and "c" refer to the quality of the astrometry as described in Sect. 2.3. Asterisks refer to the sources for which our spectroscopic data did not yield redshift (see Sect. 2.5). References to published observations are given in Sect. 3.

Article published by EDP Sciences and available at http://www.edpsciences.org/aa or http://dx.doi.org/10.1051/0004-6361:20052682

Table 1. continued.

			Radio properties			Optical properties		
IAU name[1]	RA[2]	Dec[2]	Morphology[3]	α	Flux[4]	Magnitude	z	Observations[5]
	[J 2000]	[J 2000]	(Size)		[Jy]			
1523−017 (mg)	15 26 30.99	−01 54 13.8	T (12″)	–1.04	2.07	R = 21.9 ± 0.2	0.93	I2, S1, S3, b
1612−208 (oo)	16 15 56.00	−20 58 09.3	U (<5″)	–1.22	(0.35)	R = 22.0 ± 0.2	...	I2, a, ∗
1621−196 (oo)	16 24 35.55	−19 47 15.6	T (19″)	–1.37	(0.55)	R = 21.6 ± 0.2	...	I2, a, ∗
1623−194 (oo)	16 26 24.90	−19 35 04.8	D (11″)	–1.12	0.98	R = 22.5 ± 0.2	...	I2, a, ∗
1631−222 (oo)	16 34 49.82	−22 22 11.5	U (<5″)	–1.46	4.28	R = 25.5 ± 0.4	...	I2, b
1632−199 (oo)	16 35 45.45	−20 04 18.0	SR (∼3″)	–1.05	0.96	R > 23.4	...	I2, b
1859−187 (oo)	19 02 05.59	−18 43 31.6	D (26″)	–1.39	(0.65)	R = 22.9 ± 0.2	...	I2, b
2011−169 (oo)	20 14 38.28	−16 48 21.7	SR (∼1″)	–1.05	(0.60)	R > 25.6	...	I2, a
2023−156 (oo)	20 26 42.31	−15 30 04.3	D (9″)	–1.44	(0.9)	R = 23.6 ± 0.3	...	I2, b, ∗
2057−179 (oo)	21 00 15.18	−17 45 50.7	D (10″)	–1.15	3.04	R = 21.5 ± 0.3	0.92	I5, S7, a
2105−119 (oo)	21 08 18.83	−11 41 56.2	D (∼4″)	–1.20	0.87	R = 24.3 ± 0.3	...	I2, b
2222−057 (oo)	22 25 03.91	−05 29 56.0	D (8″)	–1.16	(0.55)	R > 23	...	I5, a
2232−062 (oo)	22 35 07.87	−05 58 37.5	D (11″)	–1.10	(0.8)	R ∼ 23.5	...	I3, b
2236−039 (oo)	22 39 03.60	−03 38 57.9	R (3″)	–1.26	0.99	R ∼ 23	...	I3, b, ∗
2236−047 (oo)	22 39 32.73	−04 29 32.0	D (15″)	–1.42	2.94	R ∼ 22.3	0.55	published
2245−037 (oo)	22 47 37.16	−03 31 37.7	see text	–1.05	(0.35)	see text	...	I3, a
2347+015 (oo)	23 49 42.00	+01 50 55.2	R (∼4″)	–1.16	(0.30)	R = 22.8 ± 0.4	...	I2, a, ∗

Table 2. Optical imaging observations.

Run	Telescope	Instrument	Time span [yrs]	CCD	Pixel size [″]	No. of pixels
I1	NTT 3.5 m	EFOSC 2	1989	#05	0.2578	512 × 320
I2	ESO 3.6 m	EFOSC 1	1989–1991	#08	0.3375	1024 × 640
I3	ESO 3.6 m	EFOSC 1	1991–1993	#26	0.6094	512 × 512
I4	ESO/MPI 2.2 m	EFOSC 2	1991	#05	0.3500	512 × 320
I5	ESO/MPI 2.2 m	EFOSC 2	1991	#19	0.3340	1024 × 1024
I6	Danish 1.5 m	DFOSC	1996	Loral	0.3800	2052 × 2052

Table 3. Optical spectroscopy observations.

Run	Telescope	Instrument	CCD	Grism	Pixel size (nm)	Wavelength range (nm)
S1	ESO 3.6 m	EFOSC 1	#08	B 300	0.48	350–700
S2	ESO 3.6 m	EFOSC 1	#08	R 300	0.52	500–900
S3	ESO 3.6 m	EFOSC 1	#08	B 1000	1.3	350–1050
S4	ESO 3.6 m	EFOSC 1	#26	B 300	0.96	350–700
S5	ESO 3.6 m	EFOSC 1	#26	R 300	1.04	500–900
S6	NTT 3.5 m	EMMI	#18	#2	0.44	400–700
S7	ESO/MPI 2.2 m	EFOSC 2	#19	#1	1.0	400–920

Article published by EDP Sciences and available at http://www.edpsciences.org/aa or http://dx.doi.org/10.1051/0004-6361:20052682

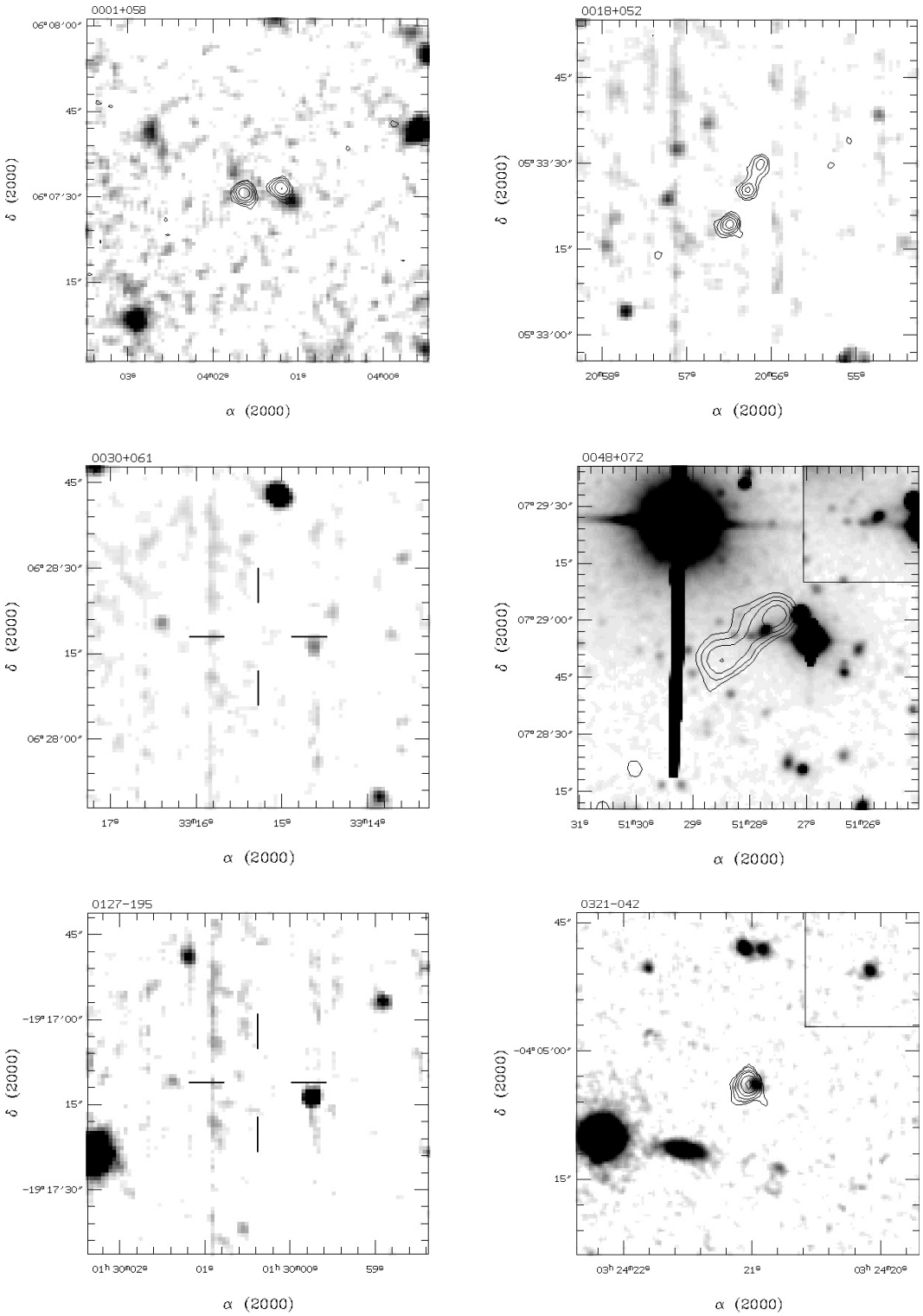

Fig. 1. Radio-optical overlays. The insets show the optical counterparts without radio contour. The radio contours are based on VLA snapshots taken at 4.8 GHz.

Article published by EDP Sciences and available at http://www.edpsciences.org/aa or http://dx.doi.org/10.1051/0004-6361:20052682

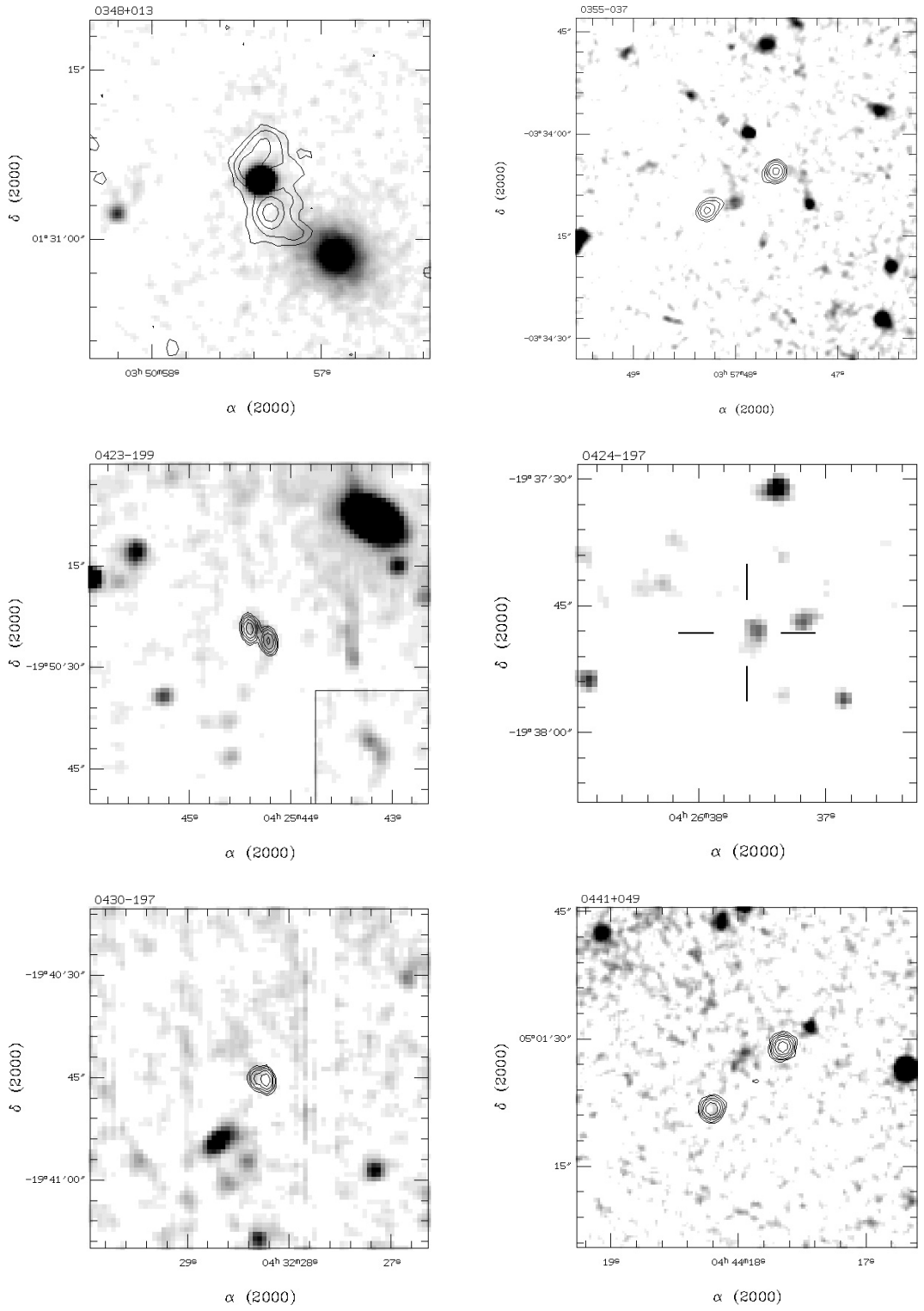

Fig. 1. continued.

Article published by EDP Sciences and available at http://www.edpsciences.org/aa or http://dx.doi.org/10.1051/0004-6361:20052682

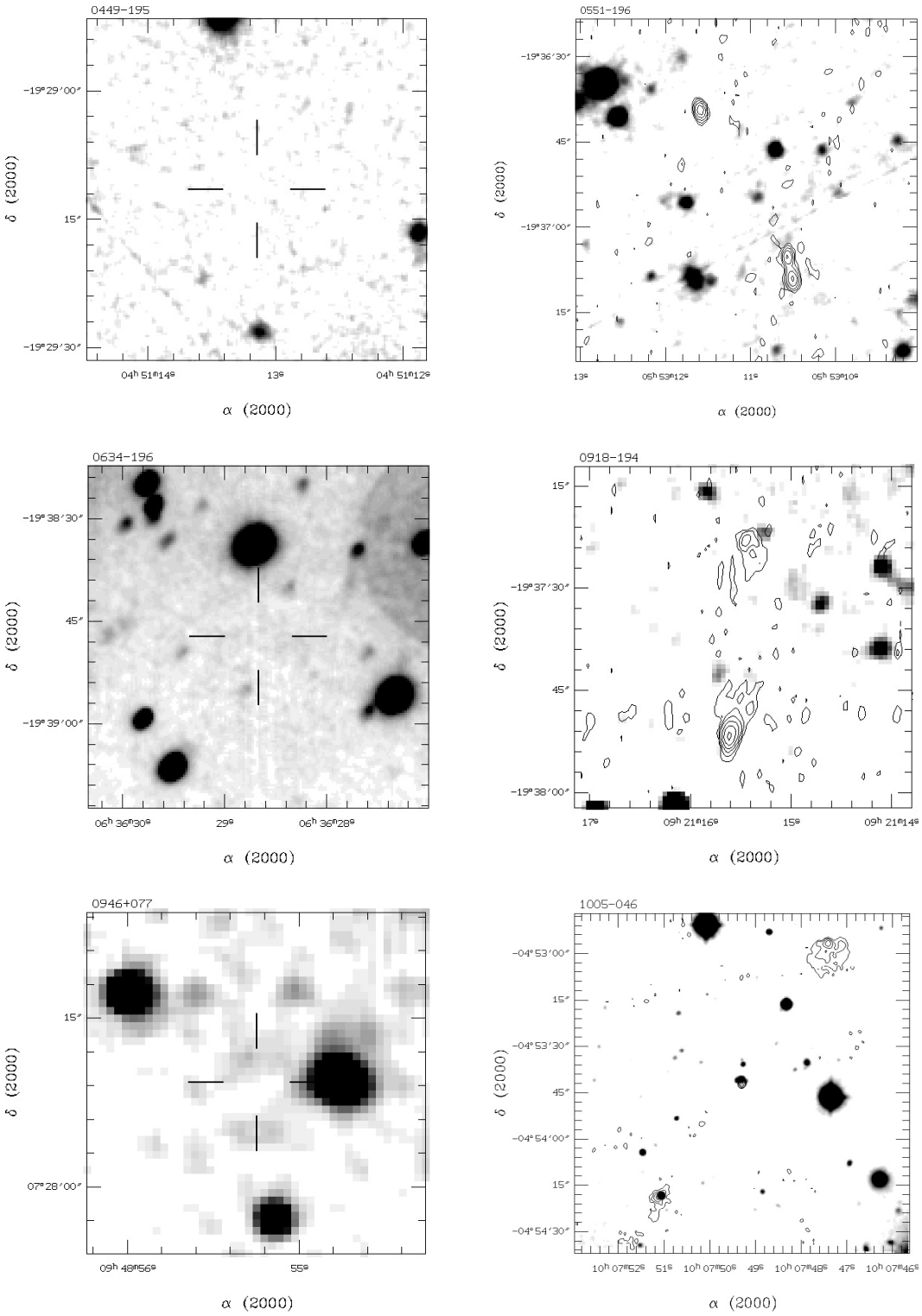

Fig. 1. continued.

Article published by EDP Sciences and available at http://www.edpsciences.org/aa or http://dx.doi.org/10.1051/0004-6361:20052682

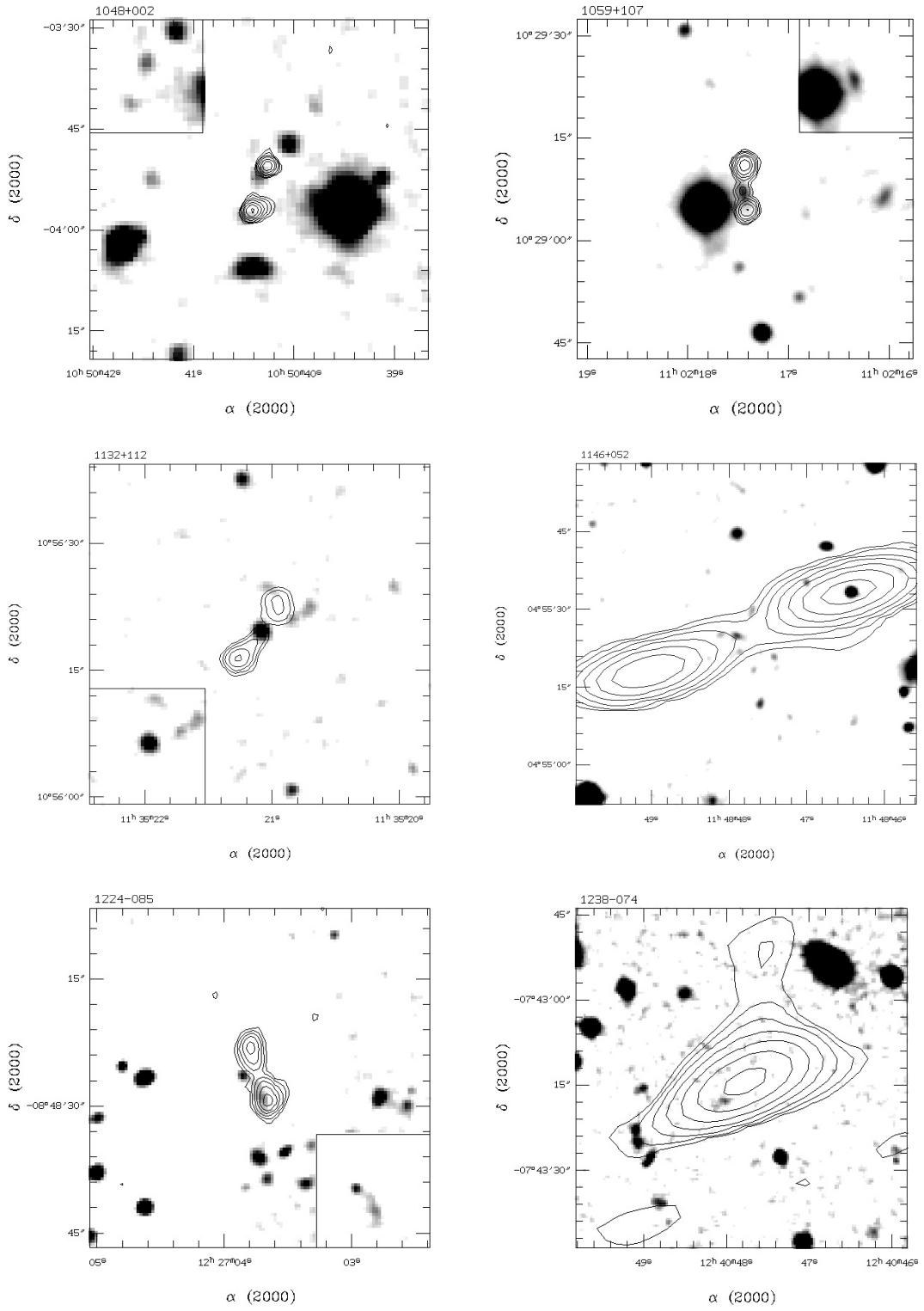

Fig. 1. continued.

Article published by EDP Sciences and available at http://www.edpsciences.org/aa or http://dx.doi.org/10.1051/0004-6361:20052682

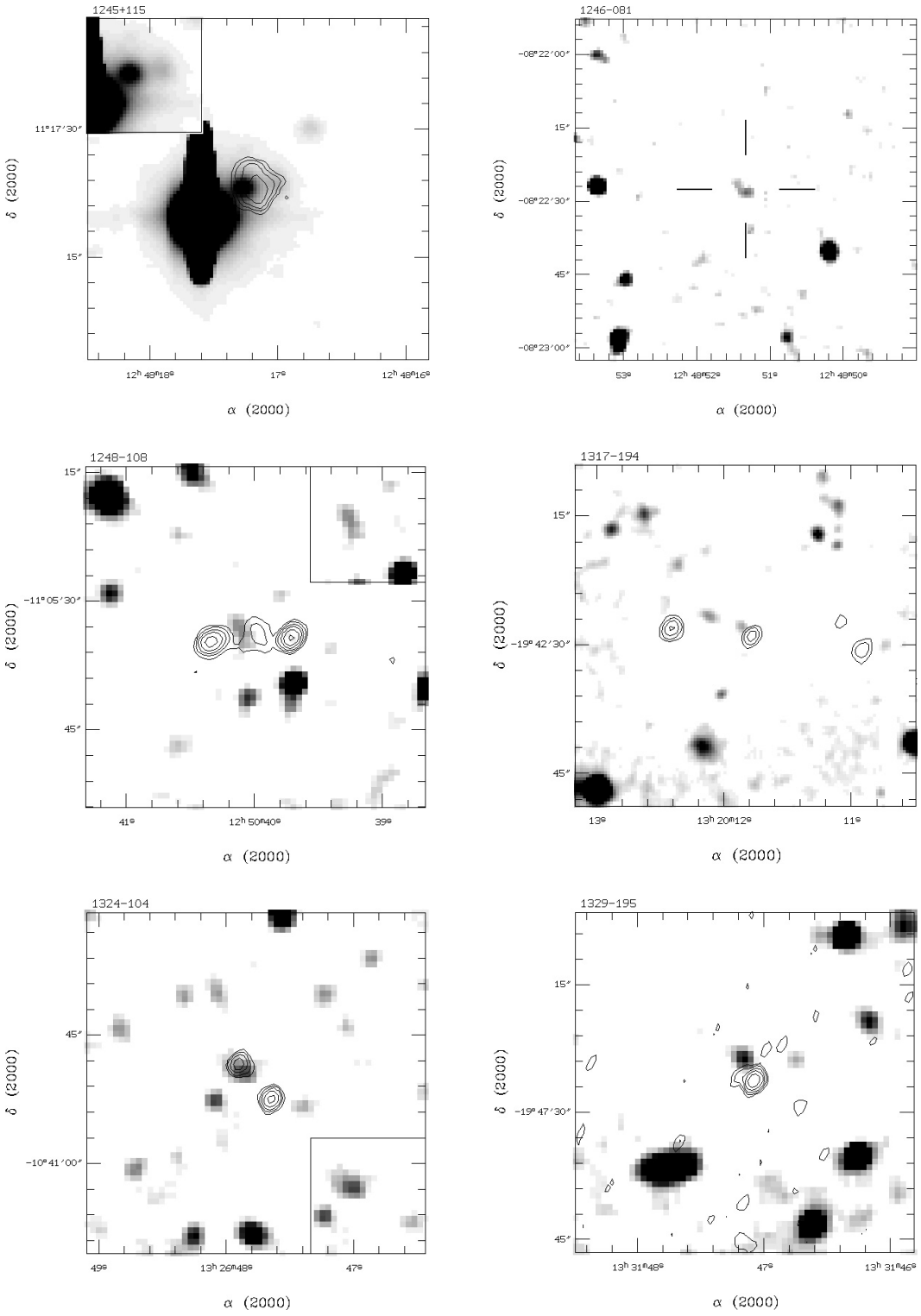

Fig. 1. continued.

Article published by EDP Sciences and available at http://www.edpsciences.org/aa or http://dx.doi.org/10.1051/0004-6361:20052682

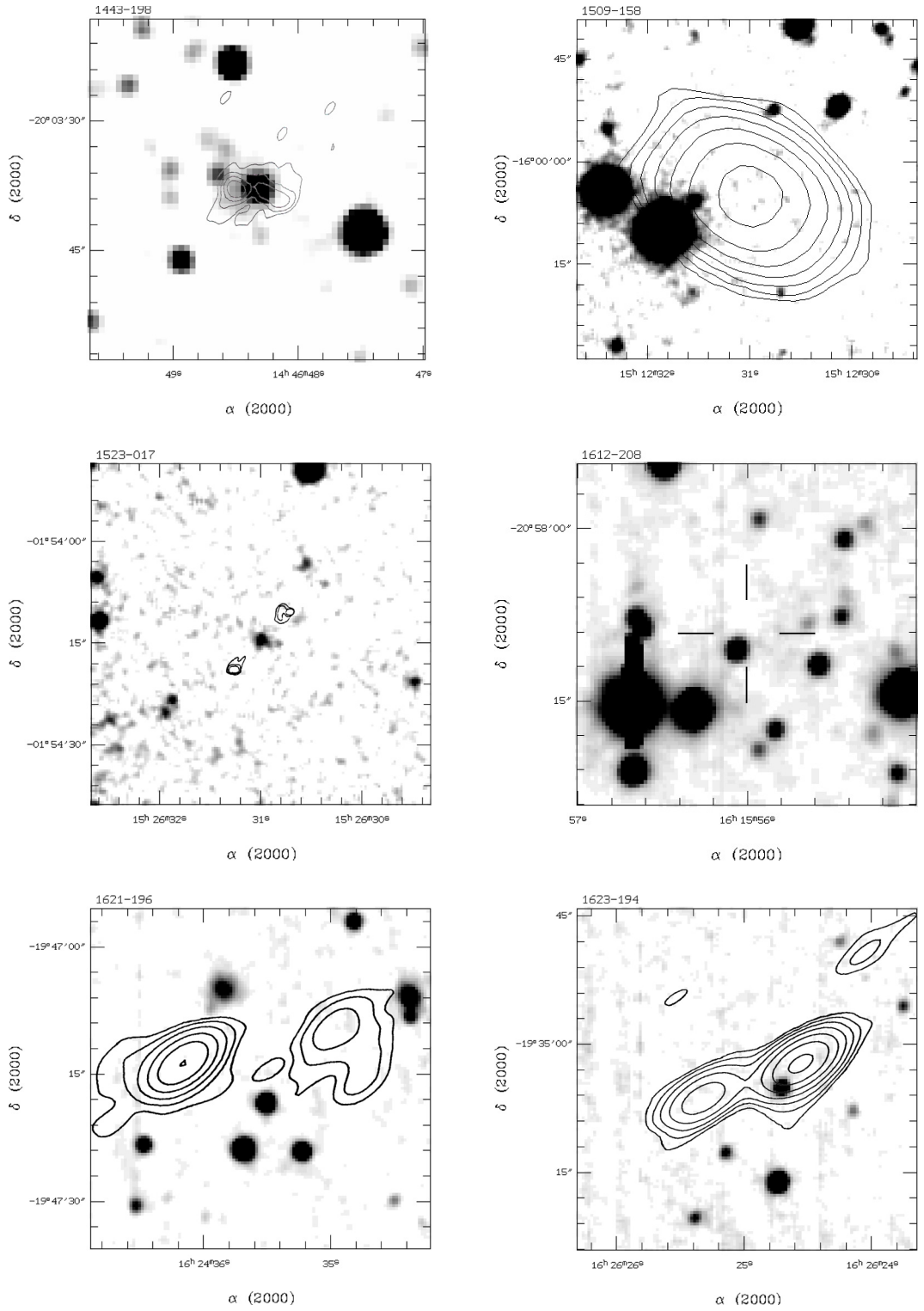

Fig. 1. continued.

Article published by EDP Sciences and available at http://www.edpsciences.org/aa or http://dx.doi.org/10.1051/0004-6361:20052682

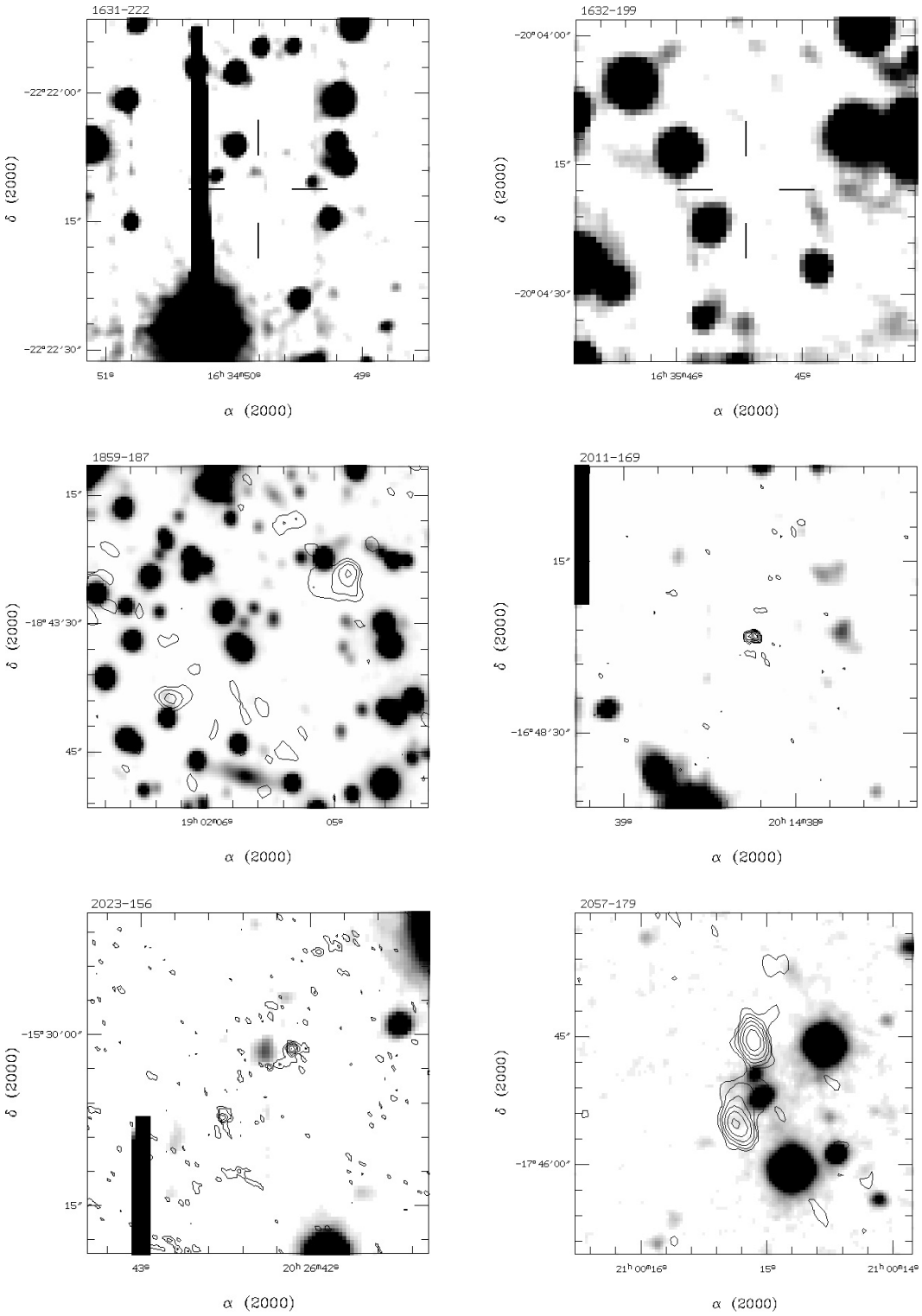

Fig. 1. continued.

Article published by EDP Sciences and available at http://www.edpsciences.org/aa or http://dx.doi.org/10.1051/0004-6361:20052682

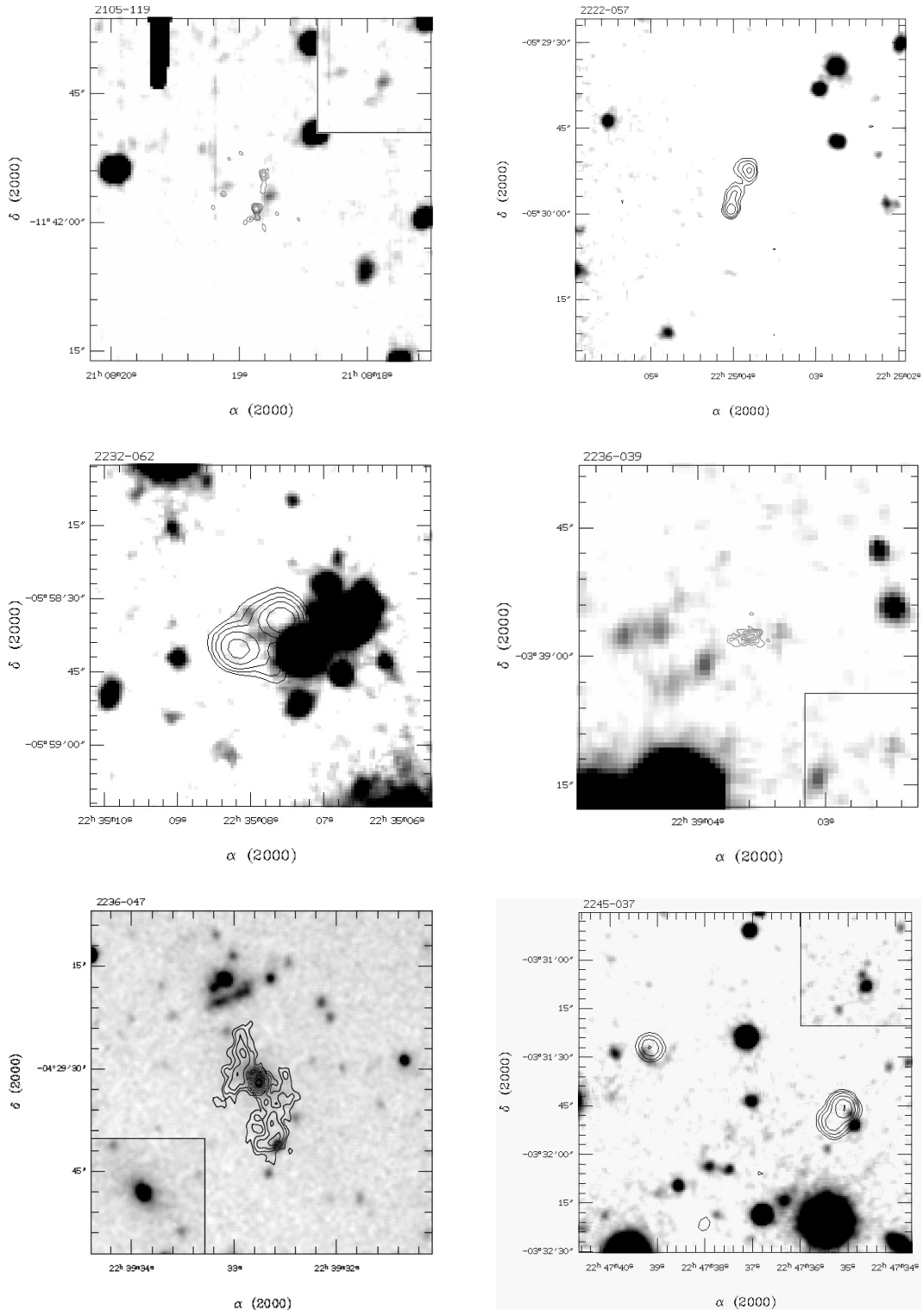

Fig. 1. continued.

Article published by EDP Sciences and available at http://www.edpsciences.org/aa or http://dx.doi.org/10.1051/0004-6361:20052682

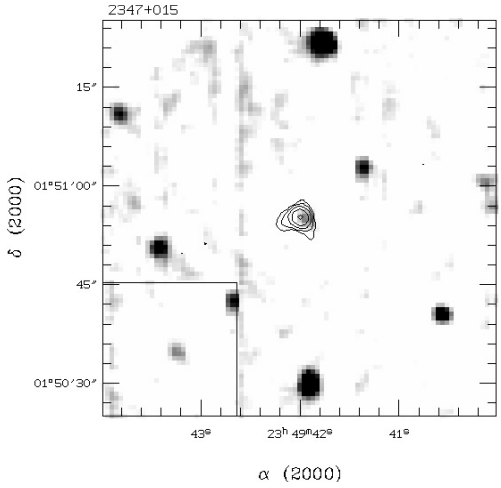

Fig. 1. continued.

Article published by EDP Sciences and available at http://www.edpsciences.org/aa or http://dx.doi.org/10.1051/0004-6361:20052682